NASA Technical Memorandum 81314

Oil-Flow Separation Patterns on an Ogive Forebody

Earl R. Keener

(NASA-TM-81314) OIL-FLOW SEPARATION PATTERNS ON AN OGIVE FOREBODY (NASA) 32 p HC A03/MF A01 CSCL 01A

N82-10011

Unclas G3/02 27728

October 1981

National Aeronautics and
Space Administration

NASA Technical Memorandum 81314

Oil-Flow Separation Patterns on an Ogive Forebody

Earl R. Keener, Ames Research Center, Moffett Field, California

National Aeronautics and
Space Administration

Ames Research Center
Moffett Field, California 94035

Oil-Flow Separation Patterns on an Ogive Forebody

Earl R. Keener*

Ames Research Center, NASA, Moffett Field, Calif.

Abstract

Oil-flow patterns on a symmetric tangent ogive forebody having a fineness ratio of 3.5 are presented for angles of attack up to 88° at a transitional Reynolds number of 0.8×10^6 (based on base diameter) and a Mach number of 0.25. Results show typical surface flow-separation patterns, the magnitude of surface flow angles, and the extent of laminar and turbulent flow for symmetric, asymmetric, and wakelike flow regimes.

Oral presentation given at the AIAA 14th Atmospheric Flight Mechanics Conference, Danvers, Mass., Aug. 11-13, 1980.

Index categories: Aerodynamics of Bodies; Aircraft Design; Missile Design; Axisymmetric Bodies; Boundary Layer Separation; Oil Flow Visualization; Subsonic Flow; Wind-Tunnel Tests.

*Research Scientist. Associate Fellow AIAA.

Introduction

Because the flight envelopes of modern aircraft and missiles include very high angles of attack, an extensive knowledge of the aerodynamics of wing and body combinations over a large range of angles of attack is required. The aerodynamics of bodies at high angles of attack is especially interesting because of the wide variety of flow phenomena that occur at those flight conditions. Several reviews of the development of the current knowledge of body aerodynamics have been presented by Chapman et al.,[1] Nielsen,[2] Spearman,[3] Ericsson and Reding,[4] and Tobak and Peake.[5,6] There are four principal flow regimes that occur[7] over the angle of attack range of bodies from 0° to 90°: 1) vortex-free flow at angles up to about 15°, 2) symmetric vortex flow at moderate angles of about 15° to 30°, 3) steady asymmetric vortex flow at higher angles of about 30° to 60°, and 4) unsteady, wakelike vortex flow at very high angles above about 60°. The most spectacular flow phenomenon is the occurrence of a large asymmetric flow separation, with a large accompanying side force when a symmetric body with a pointed nose is pitched to high angles of attack.[7-10] As the angle of attack is increased, the asymmetric flow can occur first on the aft section of the body and move forward with increasing incidence. The largest asymmetric flow and side force is likely to occur when the flow asymmetry reaches the forebody.[8] It was found that a pointed nose with a fineness ratio of 3 or more causes the largest flow asymmetry. This flow asymmetry has been suggested to be principally the effects of a hydrodynamic (inviscid) instability in the initially-symmetric vortex formation and the interaction of the vortices (which increase in strength with incidence) with the surrounding potential flow field.[10] In addition, the vortex asymmetry is also affected by boundary-layer (viscous) asymmetries caused by transition and separation differences on each side of the body. Asymmetry in either the boundary layer or

the vortex flow field on the windward surface will cause asymmetry in the other. It follows that it is of importance to understand the contribution of each of these hydrodynamically or boundary-layer-induced asymmetries on the total flow-field asymmetry.

The aerodynamic characteristics of forebody models have been investigated extensively to determine the contribution of the forebody to body aerodynamics. Force tests over a large range of Mach numbers, angles of attack, and Reynolds numbers have been reported.[6,8] Side forces were measured that are as large as 1.5 times the maximum normal force and that vary considerably with Reynolds number. Further, it was found that these side forces can be reduced or eliminated by nose bluntness, nose strakes, nose booms, or by using forebodies with fineness ratios of 2.5, or less.

In support of the force-test program, oil-flow visualization tests were made using the forebody models to determine the separation patterns in the various flow regimes. This paper presents oil-flow photographs for an ogive forebody having a fineness ratio of 3.5, at angles of attack from 0° to 90° at a Mach number of 0.25 and a Reynolds number of 0.8×10^6 (referenced to base diameter). At this Reynolds number and at high angles of attack, there is a large side force and a transitional (laminar/turbulent) boundary layer. The photographs give an indication of typical surface flow-separation patterns, the magnitude of surface flow angles, and the extent of laminar and turbulent flow for the symmetric, asymmetric, and wake-like flow-separation regimes.

Experiment

Force, oil-flow, and sublimation results were obtained in the 12-Foot Pressure Wind Tunnel at Ames Research Center at $M = 0.25$, $R_d = 0.8 \times 10^6$, and $\alpha = 0°$ to 90°. The turbulence velocity level has been measured to be less

than 0.3% of the free-stream velocity. Schlieren results were obtained in the 6- by 6-Foot Transonic Wind Tunnel at M = 0.25.

The model was an ogive forebody with a fineless ratio (ℓ/d) of 3.5 (where ℓ = length and d = base diameter). This was one of six forebody models that were tested in the investigation of forebody characteristics.[6,8] An $\ell/d = 3.5$ cylindrical afterbody, which could be clamped to the sting but which was free of the forebody, was used in some of the tests, from which it was determined that base effects did not change the basic flow characteristics.

For these oil-flow tests, the bare models were coated uniformly with a mixture of lampblack for color and motor oil of various viscosities (depending on the velocity and incidence); a few drops of oleic acid were added to the oil to ensure better dispersion of the lampblack in the oil.[11] The local aerodynamic flow forces this oil mixture into streaks that migrate in the direction of flow (skin-friction lines). The sublimination technique[11] was used to determine the position of boundary-layer transition. The models were sprayed with a saturated solution of biphenyl dissolved in trichloroethane, which is less flammable than the commonly used petroleum ether. This solution, which dries on contact with the model surface, presents a white appearance. As the wind tunnel is operated, the biphenal coating sublimes faster in regions of turbulent flow than in the regions of laminar flow. Usually, a line of demarcation can be seen between these two regions. The schlieren photographs were obtained in the 6- by 6-Foot Tunnel at M = 0.25, using a standard mercury-vapor-lamp schlieren system. The centers of the vortex cores were seen as abrupt changes in light intensity from dark to light.

Effect of Angle of Attack on Oil-Flow Patterns

The oil-flow patterns were thoroughly documanted for the ogive forebody ($\ell/d = 3.5$) at $R_d = 0.8 \times 10^6$. This Reynolds number is slightly higher than the critical Reynolds number range of 0.1×10^6 to 0.5×10^6 for a circular cylinder, so that the effects of boundary-layer transition are likely to occur. Photographs were taken at 5° increments in angle of attack to ensure that flow patterns would be obtained in each of the vortex flow regimes. Representative photographs are shown in Fig. 1 for angles of attack of 5°, 10°, 20°, 30°, 40°, 55°, 70°, and 88°. Also shown are sublimation photographs at $\alpha = 20°$ and 40°. Figure 2 presents sketches of the oil-flow patterns on the body surface as if it were "unwrapped," showing the principal features of the surface-flow patterns (skin-friction and separation lines). A key to the labels on the sketches is given in Fig. 2.

Angle of Attack: 5°

Two oil-flow photographs are shown in Fig. 1a for the left side at body meridian angles of $\theta = 135°$ and $\theta = 180°$; sketches of the flow pattern are presented in Fig. 2a for the "unwrapped" surface. First, there is a noticeable crossflow due to incidence. The angle δ_s that the local oil-flow streaks make with the free-stream flow direction was measured along the sides at $\theta = \pm 90°$. Near the nose at $x/\ell = 0.2$ (where x is the axial length from the nose tip and ℓ is the forebody length), $\delta_s \approx 24°$, which is about 2.5 times the external potential angle at the edge of the boundary layer of $\delta_e = 2\alpha = 10°$. (δ_e is determined by calculating the crossflow component of velocity (normal to the axis and parallel to the surface) at $\theta = 90°$ for a cylinder that, from potential theory, is twice the crossflow component of the free-stream velocity V_N. This velocity of $2\,V_N$ is then combined with the axial component

of the free-stream velocity, $V_\infty \cos \alpha$. The resulting flow angle is $\delta_e = 2 \tan \alpha$.) Rearward of $x/\ell = 0.2$, the flow angle δ_s decreases with increasing length until $\delta_s \approx \delta_e = 10°$ at $x/\ell \approx 0.5$ and beyond to the base.

The significantly higher oil-flow angles ahead of $x/\ell = 0.5$ must be induced by a large pressure gradient normal to the potential-flow streamlines at the edge of the boundary layer. The result is that the local velocity distribution in the boundary layer between the edge and the surface is highly skewed in the direction ahead of the inviscid streamline. This skewness increases the possibility of local boundary-layer inflectional instability (see, for example, Ref. 12) similar to that which occurs on swept wings, resulting in an array of vortices that are nearly streamwise and are submerged in the laminar boundary layer. The occurrence of these vortices is dependent on the Reynolds number and angle of sweep. On long bodies the conditions exist for the appearance of these vortices over the entire body length as soon as the body departs from zero incidence. The presence of these vortices on swept wings is known to induce early transition to a turbulent boundary layer; as a result, the presence of these vortices on the body could promote local transition to turbulence over the forward half of the forebody, where the flow is normally expected to be laminar. This is one mechanism by which the shape of the forebody can affect the local flow conditions through the distribution of crossflow angle along the length. Note that in this same forward part of the forebody the oil thickens for a short distance, forming a patch of oil (probably the accumulation of oil caused by a thickening laminar boundary layer). However, note that within the patch of oil there are regularly spaced heavy oil streaks that are at an angle to the local skin-friction lines. It is possible that these heavy oil streaks are a result of the crossflow inflectional instability (CI). Note that these streaks appear

to converge downstream, as if the flow is in the initial process of forming a "local" line of separation[6] (in which skin-friction lines coalesce from both the windward and the leeward) (see $\alpha = 10°$). Downstream of the thickened patch of oil, the oil is scrubbed (thinned) indicating that the flow is turbulent to the base. On the sides near the base it is not certain if boundary layer transition occurs; however, it is suspected that transition occurs along an oblique line that starts at the patch of oil (see Fig. 2a and the discussion for $\alpha = 20°$). On the leeward surface near the base there is no indication of reversal of the crossflow (normal) component of the direction of flow; that is, there is no crossflow separation near the base.

Angle of Attack: 10°

The oil-streak angles δ_s on the sides at $\theta = \pm 90°$ are about 41° at $x/\ell \approx 0.2$ (Fig. 1b). This is about twice the potential angle of 2α. Consequently, the boundary-layer flow continues to be highly skewed over the forward part. The patch of thickened oil that occurred at $\alpha = 5°$ develops into a wide band of oil on each side at $\alpha = 10°$, located at $\theta \approx \pm 135°$ and extending from the nose tip to $x/\ell = 0.45$, where the ends of the oil bands appear to be swept away by the crossflow behind them. The wide band of oil appears to contain heavy oil lines, similar to those at $\alpha = 5°$. Local primary laminar separation (LS) must occur at the band of oil, and reattachment (R) of the boundary layer must occur leeward of the band of oil since the oil streaks there continue toward the leeward. This pattern indicates that the band of oil marks the existence of a swept, laminar separation "bubble" ("B"). According to conical-flow concepts, local separation at the nose tip was not expected until $\alpha \geq \delta_N$, where δ_N is the nose semiapex angle of 16.5° for the $\ell/d = 3.5$ ogive. Rearward of $x/\ell = 0.45$ the band of oil does not exist and the oil is scrubbed, indicating that boundary-layer transition (T) occurs on the sides and

terminates the laminar separation bubble (Fig. 2b). The oil streaks on the lee side continue to converge slightly (as they did at $\alpha = 5°$), indicating that turbulent separation is imminent in this region.

A special comment is necessary concerning the swept laminar separation bubble ("B"). The term bubble has been used informally in the description of two-dimensional laminar separation that is followed by transition in the shear layer shortly after separation, so that the shear layer bends towards the surface and reattaches on the surface, forming an enclosed bubble. A similar oil-separation line has been observed on the leading edges of swept wings and these have also been informally called laminar-separation "bubbles," referring to their characteristic that the flow reattaches in a short distance, forming a short "bubble-like" separation region. This swept bubble-like pattern on the forebody (Fig. 1) was discussed with G. Chapman, M. Tobak, and D. Peake (Ames Research Center), who are studying the topology of these types of flows (see, for example, Refs. 5 and 6). They pointed out that there is a fundamental difference in the flow within the "bubble" between two- and three-dimensional flows. In 2-D separation, the accepted flow model is a closed circulation; streamlines within the bubble form closed paths. In 3-D separated flow there must be transverse flow parallel to the separation line. As a result of this flow, viewed in a crossflow plane (cf. sketch in Fig. 1b), the circulation zone is not closed and the projections of streamlines in this plane do not form closed paths. Instead, the bubble has the form of a growing vortex. In this paper, the informal term "swept bubble" ("B") is used to refer to this type of flow separation; however, the separation line is labeled a primary laminar separation line (LS), with the term primary referring to the fact that in the crossflow plane, the separation is being fed from boundary-layer fluid originating at the windward meridian (in contrast to secondary separation (see $\alpha \geq 20°$)).

Angle of Attack: 20°

Both an oil-flow and sublimation photograph are shown (Fig. 1c; also, refer to sketches in Fig. 2c) for the left side at $\theta = 135°$. The principal features in the oil-flow patterns are three types of primary separation. First, there is primary laminar separation (LS) in the forward [illegible] A narrow band of oil occurs at a meridian angle of $\theta \approx \pm 115°$, starting at the nose tip and ending at $x/\ell \approx 0.35$. This line of accumulated oil is a continuation of the successive stages of development of the oil pattern near the nose that led to the patch of oil at $\alpha = 5°$ and the band of oil at $\alpha = 10°$. On the windward side of each band of oil the oil-flow streaks approach the band of oil at a large angle but turn sharply downstream to converge on the band of oil. This is typical of the topology of skin-friction lines approaching a separation line. However, it is surprising that this primary laminar separation line is located at $\theta \approx \pm 115°$, which is so far from the expected angle of $\theta \approx \pm 90°$ for the separation of a laminar boundary layer. (At $\alpha = 10°$ the swept laminar separation bubble formed at even a larger body angle of $\theta \approx \pm 135°$.) Perhaps this laminar separation is delayed because of the presence of local streamwise vortices from the inflectional instability in the highly skewed boundary layer near the nose. (See the discussion of the sublimation test that follows.) It is interesting to note that in spite of the fine detail that is shown in the enlarged close-up photographs, the minute flow pattern at the nose tip is not as clearly defined as desired behind the separation line. Doubling or tripling the size of the model probably would not produce clearer results; nor is it possible to make meaningful flow-field measurements with probes or laser velocimetry close to the nose tip. Yet, it is in the area close to the nose tip that the principal flow pattern is determined for the rest of the body (see Morkovin's comments[13] on the "birth of a vortex").

Secondly, a small but very interesting region occurs at $0.2 < x/\ell < 0.35$ where two primary separation lines occur. This region is called herein primary transitional separation (TRS). It is much more prominent at $\alpha = 40°$, where it is discussed more fully.

Thirdly, primary turbulent separation (TS) occurs at $\theta \approx \pm 140°$, in the region rearward of $x/\ell \approx 0.35$, where the end of the primary laminar separation line occurs. In this region, boundary-layer transition occurs upstream (windward) of the laminar separation lines on the sides so that the laminar separation is changed to turbulent separation. This effect of boundary-layer transition is verified in the sublimination photograph in Fig. 1c. Note that the white sublimation material ends at the oil line at $x/\ell \approx 0.35$, indicating that transition occurs at this line. Rearward of $x/\ell \approx 0.35$, where the oil line disappears, the sublimation material ends along a ragged path of decreasing meridian angle to the windward.

Barely noticeable in the sublimation photographs but easily seen are striations in the sublimation material that can be seen from the base to the nose, throughout the region of the highly skewed boundary layer. The striations are oriented roughly along the same direction as the oil streaks and these striations indicate the presence of vortices that are produced in the boundary layer by crossflow inflection instability.[12]

Finally, at $\theta \approx \pm 160°$, a secondary separation line (SS) occurs which can be traced forward ahead of the nose-piece junction but not quite to the tip. Secondary separation results from the separation of the reversed leeward crossflow streaming from the line of reattachment of the primary vortex flow at $\theta = 180°$. The secondary separation is thought to be induced by the suction of the primary separation vortex located in the flow above the surface tending to

lift the boundary layer off the surface. The resulting secondary vortex rotates in a direction opposite to that of the primary vortex.

Angle of Attack: 30°

Primary laminar separation lines (LS) are clearly identified by reverse crossflow in the leeward oil-flow streaks (Fig. 1d; also Fig. 2d). They extend from the nose tip to $x/\ell = 0.60$ and are located at $\theta \approx \pm 110°$. The region for the simultaneous occurrence of two primary separation lines [primary transitional separation (TRS)] moves slightly rearward to $0.4 < x/\ell < 0.65$ at $\alpha = 30°$. (See following paragraphs on $\alpha = 40°$ for a description of this flow pattern.) Primary turbulent separation (TS) occurs over the rearward 40% length at $\theta \approx 140°$. Secondary separation occurs at $\theta \approx \pm 160°$ over the full length of the forebody.

Angle of Attack: 40°

At this test condition, four of the five principal types of flow separation that were found in the study are very prominent and are labeled in the oil-flow photograph shown for $\theta = 135°$ (Fig. 1e). Also shown is a sublimation photograph for $\theta = 135°$ showing the location of boundary-layer transition. Three types of primary separation patterns occur: 1) laminar, 2) "transitional," and 3) turbulent. These patterns appear at the lower angles but the transitional pattern is not as prominent as at $\alpha = 40°$. Secondary separation is the fourth principal separation pattern seen at $\alpha = 40°$.

Primary laminar separation (LS) (Fig. 1e; also Fig. 2e) is indicated by the oil line that occurs at $\theta \approx \pm 100°$. Region (1) (regions are designated by circled numbers in Fig. 1e) for primary laminar separation is shown to occur from the tip back to $x/\ell \approx 0.3$. However, note that the laminar separation line extends to $x/\ell \approx 0.8$ and that the region of $0.3 < x/\ell < 0.8$ is

labeled region (2). In this region two primary separation lines occur. This same flow pattern was noted at $\alpha = 20°$ and $30°$ for small regions; however, at $\alpha = 40°$ this flow pattern is prominent and extensive. This region (2) has been herein termed primary transitional separation (TRS), and it consists of primary laminar separation, followed by boundary-layer transition and reattachment, and finally, primary turbulent separation. "Transitional" is intended to mean that this pattern is transitional between the primary laminar and primary turbulent separation patterns. Although this pattern is not so well known in 2-D cylinder flows, Jones et al.[14] show an oil-flow pattern at $R_d = 1.6 \times 10^6$, similar to that of region (2), having two primary separations — laminar and turbulent. This separation pattern is the next natural hierarchy of flow separation, with increasing Reynolds number following laminar separation. It occurs when the local Reynolds number is high enough that transition occurs in a short distance following laminar separation.

Primary turbulent separation (TS), region (3) in Figs. 1e and 2e, occurs when transition moves upstream as a result of the higher local Reynolds number for the larger diameter of the rear section, eliminating the primary laminar separation and "swept bubble." Consequently, the turbulent flow remains attached until $\theta \simeq 140°$, where primary turbulent separation occurs. The sublimation photograph verifies that transition occurs along the lee of the "swept bubble" and eliminates it by moving upstream at the rear of the forebody. Also, striations were seen in the sublimation material from the base forward to $x/\ell \simeq 0.2$, which indicate the presence of vortices from crossflow inflectional instability. Note that region (3) (TS) is prominent for $\alpha = 30°$ but is greatly reduced at $\alpha = 40°$ by the increasing length of transitional separation. This verifies that the effective Reynolds number for the boundary layer is lower for $\alpha = 40°$ than for $\alpha = 30°$ (as discussed in Ref. 3),

because the effective boundary-layer length of run is lower for $\alpha = 40°$ than for $\alpha = 30°$.

The last feature in Fig. 2e is the secondary separation (SS) line (4) that occurs on the lee of the primary separation line at $\theta \approx \pm 160°$ and extends to the nose tip. In this type of flow pattern, the flow from the primary flow field circulates to the lee surface around the primary separation vortex, reattaches at $\theta = 180°$, flows toward $\theta = 160°$, where the flow separates again into a vortex filament that circulates in the opposite direction to the primary vortex. In addition, smaller vortices are possible that serve as nature's "roller bearings" in fluid separation flows.

Finally, the first small flow asymmetry appears in the leeward oil-flow pattern in the secondary separation line (see sketch in Fig. 2e). As a result, a small measured side force occurs ($C_Y = 0.5$).

Angle of Attack: 55°

All of the features of the oil-flow pattern are asymmetric, and a large, relatively steady asymmetric force of $C_Y = 2.6$ (Figs. 1f and 2f) was measured. Although the flow has some unsteadiness, the unsteadiness does not predominate. Note that vortex traces are shown as sketched from schlieren photographs. These vortices are highly asymmetric and slightly unsteady but do not switch position. The first vortex is shed near the nose tip and passes high above the forebody almost straight back from the nose tip. The second vortex is located close to the surface and disappears at mid-length.

The primary laminar separation lines (LS) extend the full length on both sides but are asymmetrically located at $\theta \approx -100°$ on the right side and $\theta \approx 80°$ on the left, which is correct for a right-side force. Primary transitional separation (TRS) is clearly indicated on the right side, starting at $x/\ell \approx 0.2$, by the overlapping primary laminar separation (LS) and turbulent separation (TS)

lines. On the left side, the turbulent separation line extends ahead to $x/\ell \simeq 0.4$, compared with its extension to about 0.2 on the left, so that the transitional separation is asymmetrically disposed longitudinally as well as circumferentially. In addition, the secondary separation lines (SS) on the lee are very asymmetric. The right separation line extends at least to the midlength, where it is close to the top centerline. Consequently, the right-hand vortex lines cross over the lee centerline to the left side and disappear at $x/\ell \simeq 0.5$. The left secondary separation line is pushed to the left side to $\theta \simeq 140°$. This oil line seems to branch into several lines at $x/\ell \simeq 0.3$, near the location where the first vortex is shed (in the sketch). Sometimes it is stated that a vortex sheet "tears" when it is shed; however, from topological considerations,[5] vortices cannot "tear" but rather the sheet must be continuous. Also, separation lines do not end abruptly but must originate and terminate at a nodal point, saddle point, or focus. There has to be a continuity to the vortex structure and the accompanying separation lines. In addition, a new vortex must form on the left side where the first vortex is shed; however, this is also not clear in the oil-flow pattern. Consequently, it is felt that the topology of these patterns at $\alpha = 55°$ is still not fully understood.

Sublimation photographs (not shown) show striations on the windward surface from the base forward to near the nose, indicating that crossflow inflectional instability also occurs at this angle.

Angle of Attack: 70°

The oil-flow pattern exhibits a small asymmetry on the lee which is considerably reduced from that at $\alpha = 55°$; however, the laminar separation on each side is symmetric (Figs. 1g and 2g). A prominent difference from the pattern at $\alpha = 55°$ occurs on the leeward surface over the rear half, where the oil accumulates into a large dark patch with no flow lines. From this flow

pattern and from those at $\alpha = 80°$ and 88°, it is certain that in the region of the rear half the flow separates into an unsteady, wake-like flow, similar to that behind a swept circular cylinder. In such a flow the vortices leave the surface on each side in an alternating pattern that could be either periodic (like a vortex sheet) or random, depending on the Reynolds number.

Angle of Attack: 88°

The accumulated patch of oil on the lee indicates wake-like separation extending forward to the nose tip (Figs. 1h and 2h). The side force is zero for this angle. Note that the flow separation on the sides is transitional forward to $x/\ell \approx 0.2$. At $R = 0.8 \times 10^6$ the boundary-layer flow should be supercritical, and hence a length of turbulent separation was expected near the base.

Measured Surface Flow Angles

Figure 3 presents the measured surface oil-streak angles (skin-friction-line angles) at $\theta = \pm 90°$ on the sides of the $\ell/d = 3.5$ ogive and of the 20° cone. Data for the 20° cone at $\alpha = 36°$ are also included for comparison. As mentioned previously in the discussion of the oil-flow patterns, the angles near the nose at $\alpha = 5°$ and 10° are about 5 α, which is more than twice the potential-flow angle of 2 α at low angles of attack; this indicates that the boundary-layer velocity profiles are highly skewed near the nose. Further, it is interesting that with increasing angle of attack, the flow angle δ_s follows close to the curve for $\tan^{-1}(5 \tan \alpha)$. Rearward of the nose, the flow angle decreases with increasing distance from the nose, until, over the rear half of the forebody, the oil-flow angles are close to the potential-flow angle of $\tan^{-1}(2 \tan \alpha)$. Between $\alpha = 40°$ and 70° the flow angles on each side are asymmetric because of the asymmetry in the vortex flow field (see cross-hatched

region in Fig. 3). Note that most of the curves have inflections near $\alpha = 20°$ and 40°. These angles are close to the onset of symmetric and asymmetric vortex flow, respectively, and these inflections represent a retardation in rate of change in surface-flow angle with incidence. Evidently, a strong favorable crossflow pressure gradient is responsible for the increase in flow angle with increasing incidence and the resulting skewing of the boundary-layer velocity profiles. Therefore, the inflections in the δ_s versus α curves must result from changes in the variation of the crossflow pressure gradient with incidence, caused by the onset of the formation of the symmetric vortex flow field and, at higher incidence, by the onset of vortex asymmetry.

The data for the 20° cone at $\alpha = 36°$ (Fig. 3) show a much smaller variation with cone length than for the ogive forebody; hence, the flow is more conical than for the ogive with respect to the surface-flow angles. The measured angle for the cone is about 70°, which lies between the potential flow angle of about 56° and the skewed-flow angle of about 73° that occurs on the nose of the ogive. Therefore, the cone-surface flow angles are greatly skewed from the potential over most of the cone length. The highly skewed boundary layer has the potential of inducing inflectional instability in the velocity profiles and promoting transition, as the oil-flow patterns indicated at $\alpha = 5°$. The occurrence of inflectional instability was verified by sublimation tests at $\alpha = 20°$, 40°, and 55°, in which striations appeared on the windward surface in the sublimation materials. Thus, the difference in surface-flow angles between the cone and the ogive is one means by which the shape of the forebody can affect the local flow conditions through the distribution of crossflow velocity profiles.

Concluding Remarks

Oil-flow, sublimation, and schlieren flow-visualization tests about ogival ($\ell/d = 3.5$) and conical forebodies were conducted at a Mach number of 0.25 over an angle of attack range from 0° to 90°.

The Reynolds number of 0.8×10^6 was selected because at this Reynolds number an interesting mixture of laminar and turbulent boundary-layer flow patterns exist, and there is a large side force at high incidence. The oil-flow photographs show the surface-flow patterns that exist in the four principal flow regimes: 1) unseparated, potential, free-vortex flow; 2) symmetric vortex flow; 3) asymmetric vortex flow; and 4) wake-like, unsteady vortex flow. Symmetric vortex flow can be detected between angles of attack of 15° and 20°, starting at the base and moving forward with increasing angle of attack. Asymmetric vortex flow is seen over the rear half at $\alpha = 40°$ and spreads to the nose tip at $\alpha = 90°$.

Three types of primary separation patterns were found along the length of the forebody; they occur because of the influence of boundary-layer transition. First, primary laminar separation occurs near the nose. Second, primary transitional separation, occurs near the midsection; this type of separation pattern consists of the combination of the laminar separation, turbulent reattachment, and turbulent separation. Finally, primary turbulent separation occurs over the rear half of the forebody. The extent of these three types of primary separation depends on angle of attack. As the angle of attack increases, the region of primary transitional separation increases in length from a short length at the midsection at $\alpha = 20°$ to a long length extending to the base at $\alpha = 55°$, thus reducing the length of the primary turbulent separation to zero at $\alpha = 55°$. This reduction in primary turbulent separation with increasing incidence is clear evidence that the effective Reynolds number for the boundary

layer is lower at the higher angles of attack, a result of the decreasing effective boundary-layer length of run as angle of attack increases.

An interesting and unexpected flow pattern occurs at angles of attack near 10°. On the forward half of the forebody, where potential flow was expected, laminar separation occurred, followed by turbulent reattachment, forming a swept bubble-like flow.

Another interesting effect is the large skewing in the boundary-layer velocity profiles near the nose, resulting from the surprisingly large surface-flow angles near the nose tip. At low incidence these angles are more than twice the potential flow angle of 2α at the edge of the boundary layer on each side. This large skewing of the boundary-layer velocity profiles has the potential of inducing inflectional instability, which promotes transition and the reattachment of the flow following laminar separation. The occurrence of crossflow inflectional instability was verified at angles of attack of 20°, 40°, and 55° by sublimation tests in which striations that result from the presence of an array of vortices that are produced by the instability were observed. The skewing decreases to zero over the rear half of the ogives, but not for the 20° cone, which indicates that forebody shape influences this phenomenon.

Acknowledgments

The author would like to thank Dr. Gary Chapman and Mr. Murray Tobak of Ames Research Center for several important contributions to the analysis of the flow-visualization results.

References

[1]Chapman, G. T., Keener, E. R., and Malcolm, G. N., "Asymmetric Aerodynamic Forces on Aircraft Forebodies at High Angles of Attack — Some Design Guides," AGARD-CP-99, Stall-Spin Problems of Military Aircraft, Nov. 1976.

[2]Nielsen, J. N., "Nonlinearities in Missile Aerodynamics," AIAA Paper 78-20, Jan. 1978.

[3]Spearman, M. L., "Historical Development of Worldwide Guided Missiles," AIAA Paper 78-210, Jan. 1978.

[4]Ericsson, L. E. and Reding, J. P., "Vortex-Induced Asymmetric Loads in 2-D and 3-D Flows," AIAA Paper 80-0181, Jan. 1980.

[5]Tobak, M. and Peake, D. J., "Topology of Two-Dimensional and Three-Dimensional Separated Flows," AIAA Paper 79-1480, July 1979.

[6]Tobak, Murray and Peake, David J., "Topology of Three-Dimensional Separated Flows," NASA TM-81294, 1981.

[7]Keener, Earl R., Chapman, Gary T., and Kruse, Robert L., "Effects of Mach Number and Afterbody Length of Onset of Asymmetric Forces on Bodies at Zero Sideslip and High Angles of Attack," AIAA Paper 76-66, Jan. 1976.

[8]Kruse, R. L., Keener, E. R., Chapman, G. T., and Claser, G., "Investigation of the Asymmetric Aerodynamic Characteristics of Cylindrical Bodies of Revolution with Variations in Nose Geometry and Rotational Orientation at Angles of Attack to 58° and Mach Numbers to 2," NASA TM-78533, 1979.

[9]Keener, E. R. and Chapman, G. T., "Onset of Aerodynamic Side Forces at Zero Sideslip on Symmetric Forebodies at High Angles of Attack," AIAA Paper 74-770, 1974.

[10]Keener, Earl R. and Chapman, Gary T., "Similarity in Vortex Asymmetries over Slender Bodies and Wings," AIAA Journal, Vol. 15, No. 9, Sept. 1977, pp. 1370-1372.

[11]Maltby, R. L., "Flow Visualization in Wind Tunnels Using Indicators," AGARDograph 70, Apr. 1962.

[12]Chapman, G. T., "Some Effects of Leading-Edge Sweep on Boundary-Layer Transition at Supersonic Speeds," NASA TN D-1705, 1961.

[13]Morkovin, M. V., Prepared Comment to "Some Sources of Ground-Wind Loads in Launch Vehicles," Bound volume of papers for AIAA 5th Annual Structures and Materials Conference, Apr. 1-3, 1964.

[14]Jones, G. W., Jr., Cincotta, J. J., and Walker, R. W., "Aerodynamic Forces on a Stationary and Oscillatory Circular Cylinder at High Reynolds Numbers," NASA TR R-300, 1979.

[15]Jorgensen, L. H., "Prediction of Static Aerodynamic Characteristics for Slender Bodies Alone and with Lifting Surfaces to Very High Angles of Attack," NASA TR R-474, 1977.

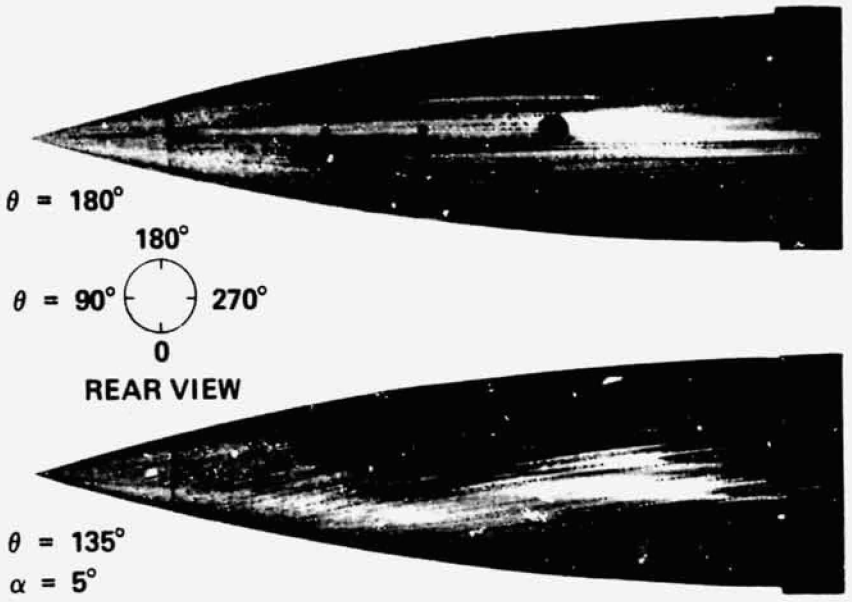

(a) VORTEX-FREE FLOW

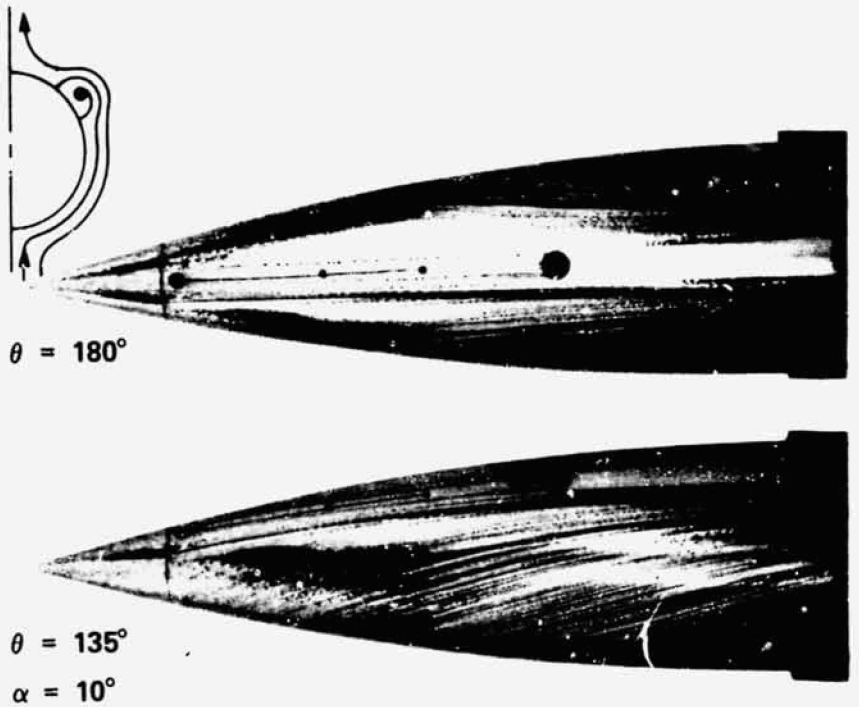

(b) LAMINAR SEPARATION "SWEPT BUBBLE"

Figure 1.- Oil-flow photographs showing the effect of angle of attack at a transitional Reynolds number of $R_d = 0.8 \times 10^6$, M = 0.25, $\ell/d = 3.5$ ogive.

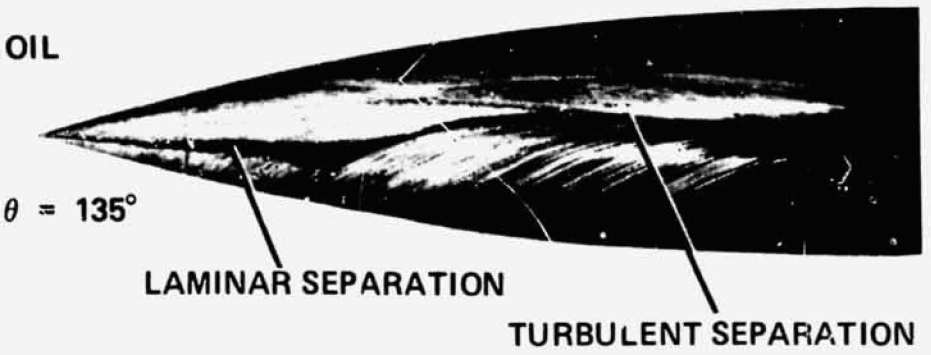

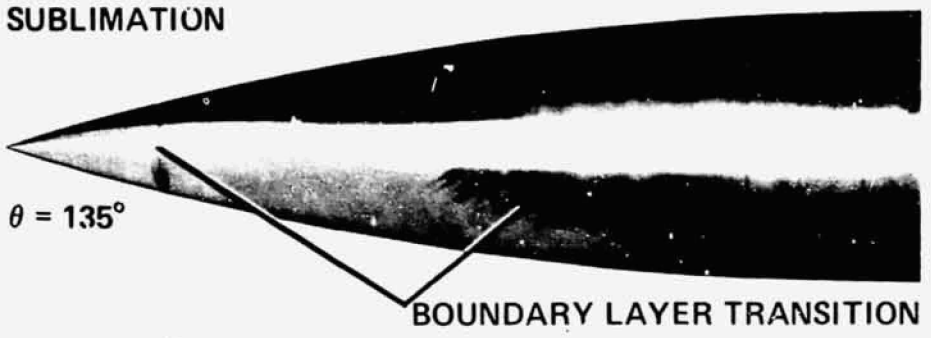

α = 20°

(c) SYMMETRIC VORTEX FLOW

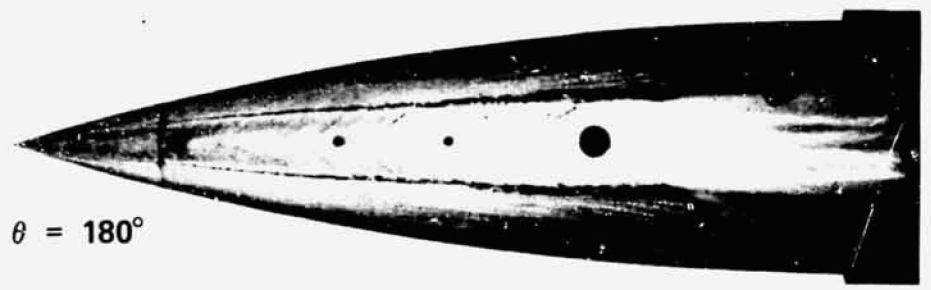

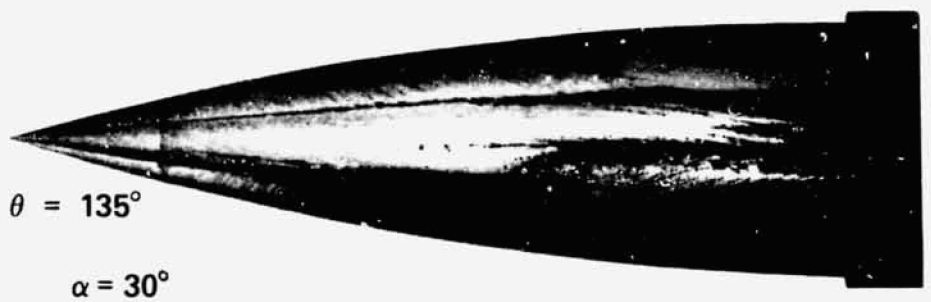

α = 30°

(d) SYMMETRIC VORTEX FLOW

Figure 1.- Continued.

ORIGINAL PAGE IS
OF POOR QUALITY

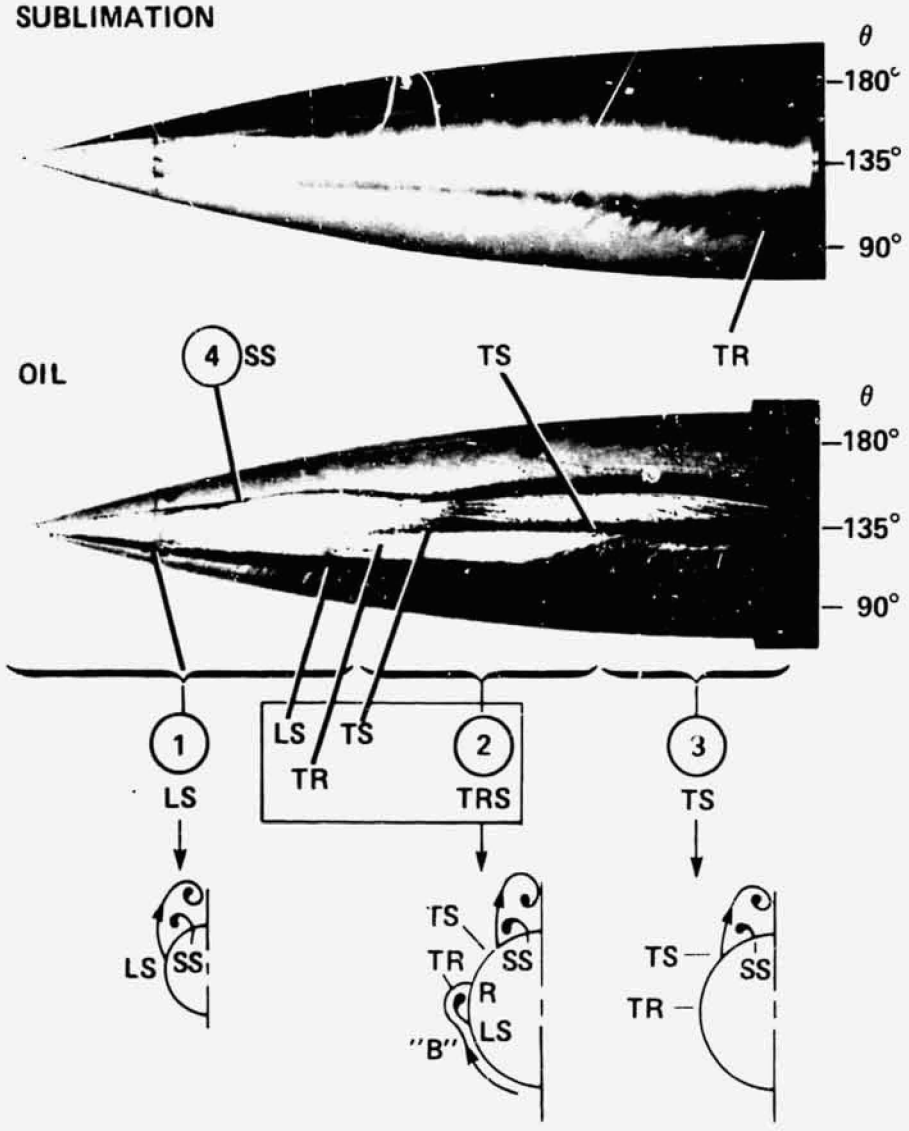

PRINCIPAL FEATURES:

1. PRIMARY LAMINAR SEPARATION, LS
2. PRIMARY TRANSITIONAL SEPARATION, TRS = (LS + TR + R + TS)
3. PRIMARY TURBULENT SEPARATION, TS
4. SECONDARY SEPARATION, SS

$\alpha = 40°$, $C_Y = 0.5$

(e) SLIGHTLY ASYMMETRIC VORTEX FLOW

ORIGINAL PAGE IS
OF POOR QUALITY

Figure 1.- Continued.

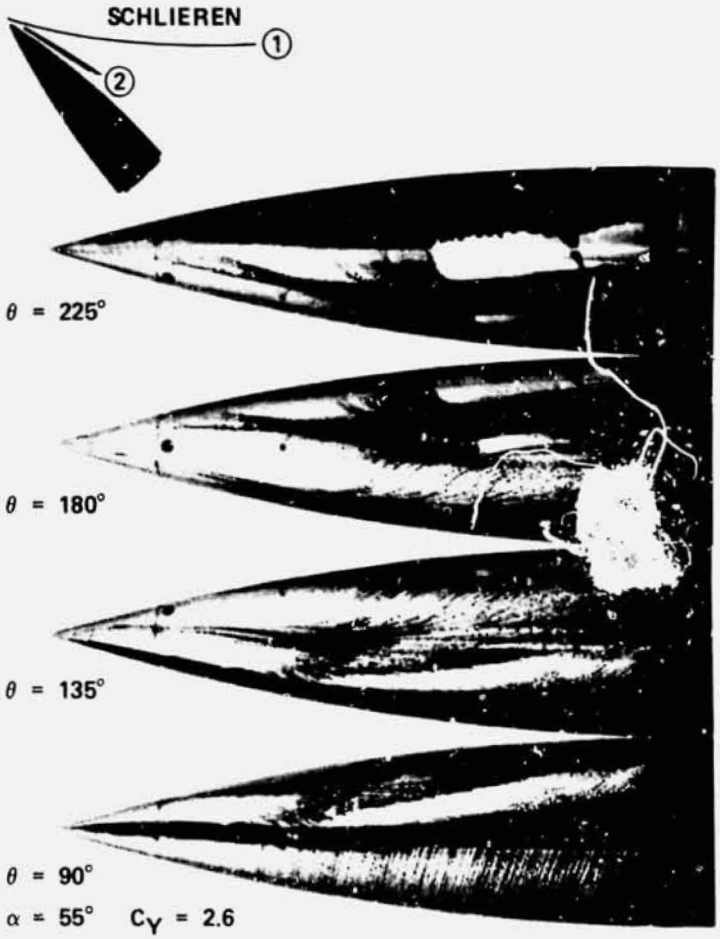

(f) ASYMMETRIC VORTEX FLOW

(g) PARTIAL WAKE-LIKE FLOW

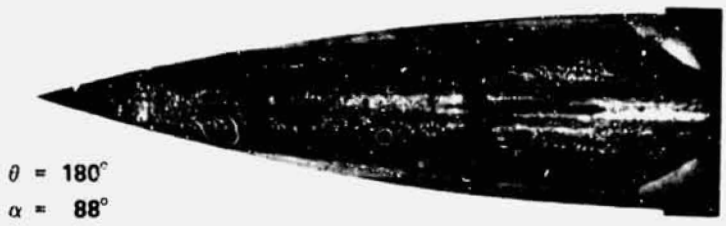

(h) UNSTEADY WAKE-LIKE VORTEX FLOW

Figure 1.- Concluded.

KEY TO SURFACE FLOW NOTATION:

L,T	= LAMINAR AND TURBULENT BOUNDARY LAYER
CI	= CROSSFLOW INSTABILITY
TR(⩘)	= BOUNDARY LAYER TRANSITION FROM SUBLIMATION TESTS
TRS	= TRANSITIONAL SEPARATION PATTERN
LS, TS	= PRIMARY LAMINAR AND TURBULENT SEPARATION
"B"	= SWEPT, 3-D, LAMINAR SEPARATION "BUBBLE"
R	= TURBULENT REATTACHMENT
SS	= SECONDARY SEPARATION
?	= UNCERTAIN, CONJECTURE

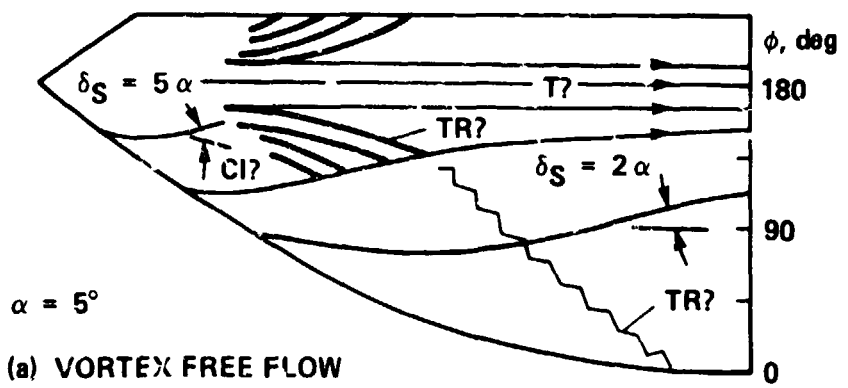

(a) VORTEX FREE FLOW

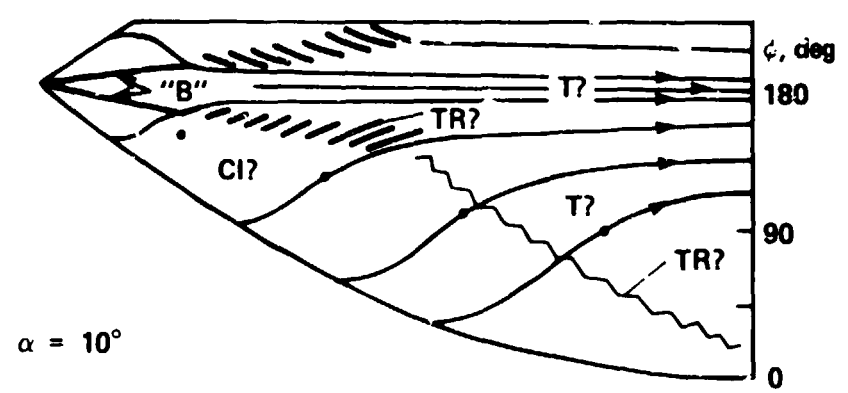

(b) LAMINAR SEPARATION "SWEPT BUBBLE"

Figure 2.- Sketches of oil-flow patterns (Fig. 1) showing the effect of angle of attack at a transitional Reynolds number of $R_d = 0.8 \times 10^6$, M = 0.25, ℓ/d = 3.5 ogive.

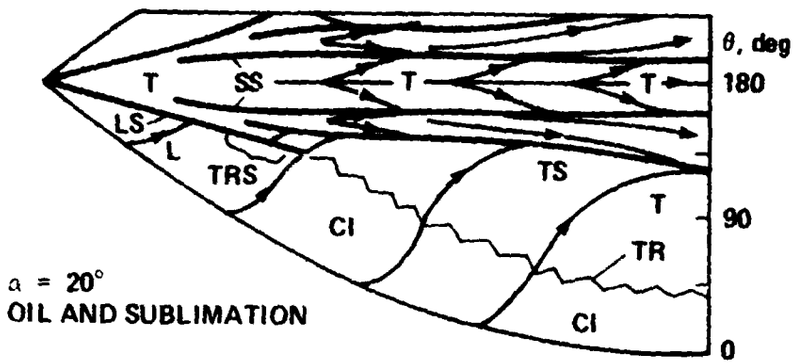

(c) SYMMETRIC VORTEX FLOW

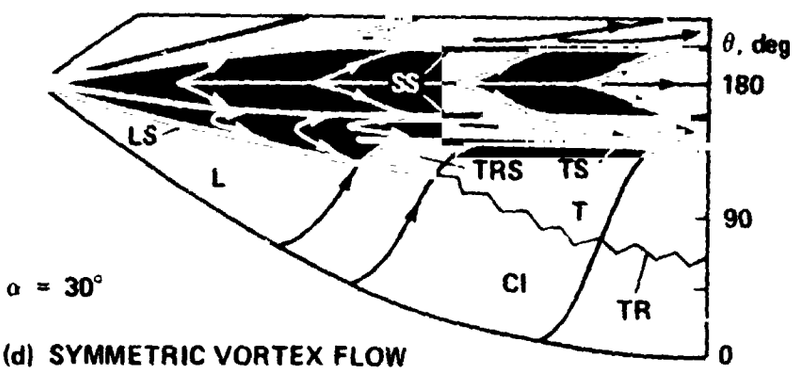

(d) SYMMETRIC VORTEX FLOW

Figure 2.- Continued.

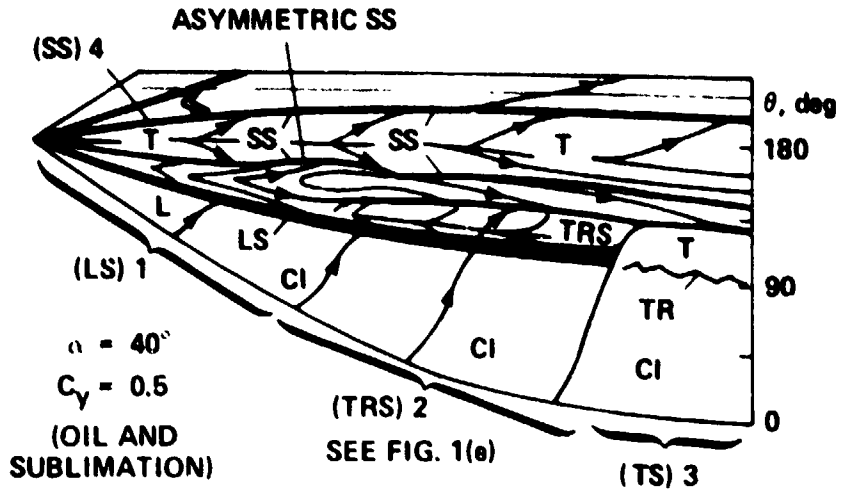

(e) SLIGHTLY ASYMMETRIC VORTEX FLOW

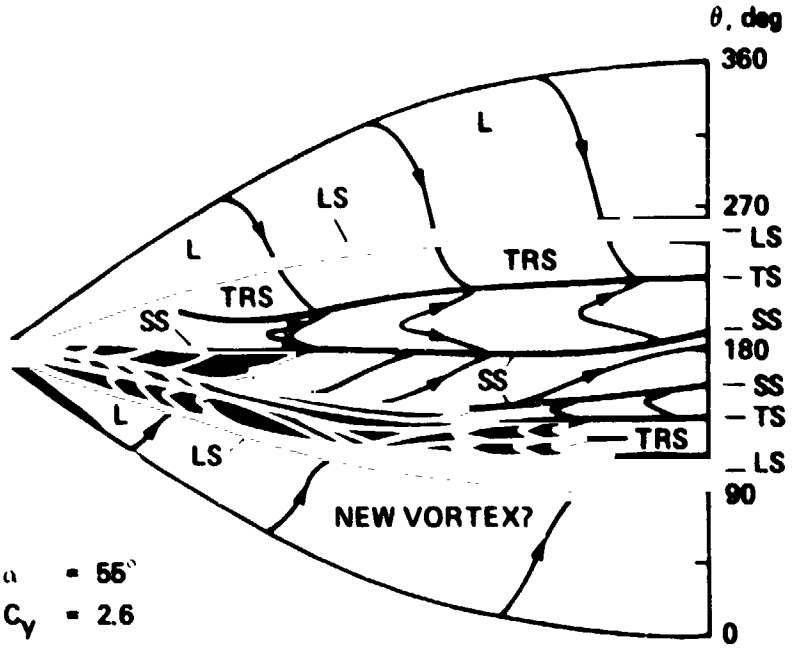

(f) ASYMMETRIC VORTEX FLOW

Figure 7.- Continued.

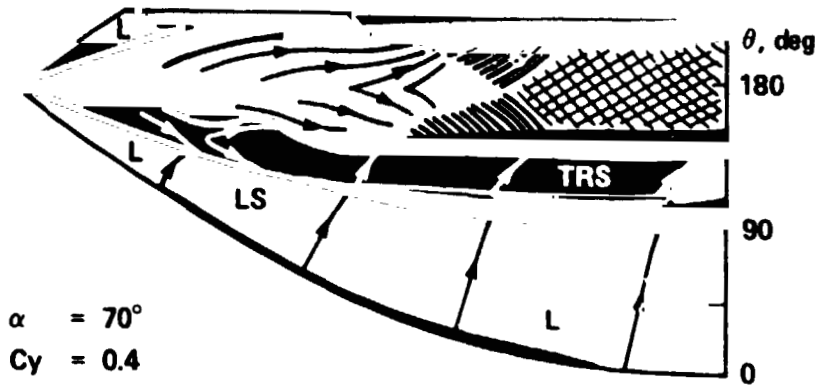

(g) PARTIAL WAKE-LIKE FLOW

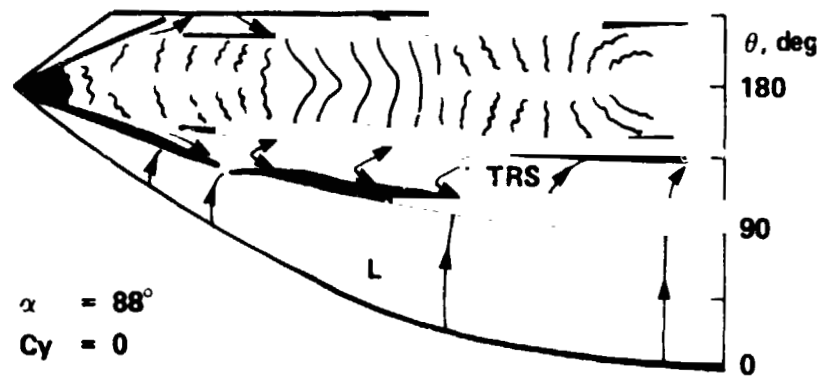

(h) UNSTEADY WAKE-LIKE VORTEX FLOW

Figure 2.- Concluded.

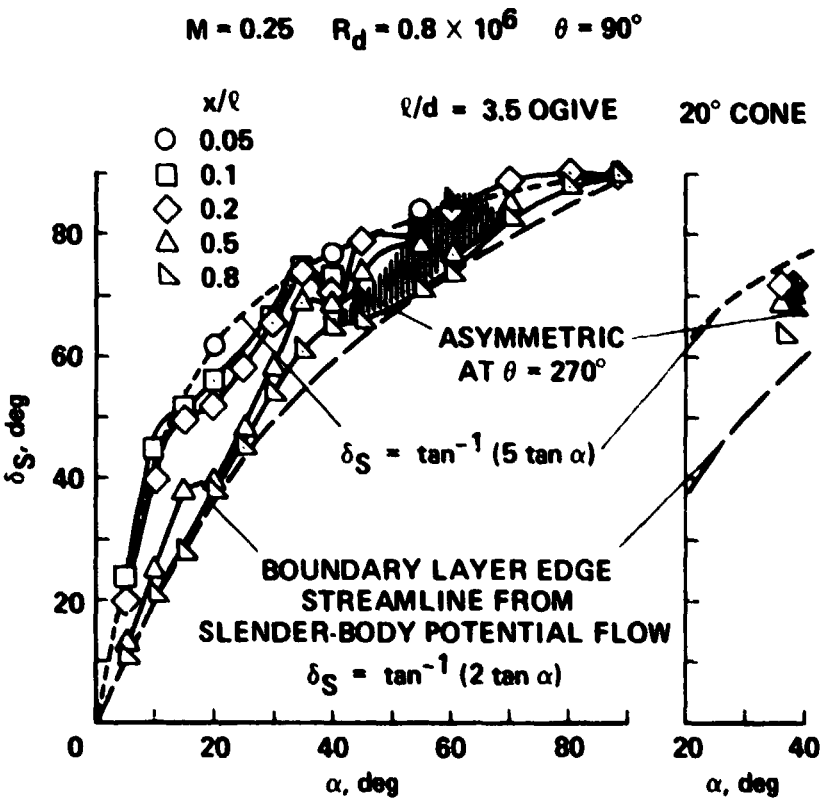

Figure 3.- Surface oil-flow (skin-friction line) angles on the sides of two forebody models.